Catalysis Science & Technology

Accepted Manuscript

ROYAL SOCIETY OF CHEMISTRY

www.rsc.org/catalysis

Catalysis Science & Technology

RSCPublishing

ARTICLE

Temperature Pretreatment Effects on Propane Cracking over H-SSZ-13 Zeolites

Cite this: DOI: 10.1039/x0xx00000x

J.H. Yun [a] and R.F. Lobo [a] *

Received ooth January 2012,
Accepted ooth January 2012

DOI: 10.1039/x0xx00000x

www.rsc.org/

The effect of thermal treatment of SSZ-13 on catalytic activity has been investigated by using a monomolecular propane conversion as a probe reaction. Two samples with Si/Al ratios of 12 and 6 were prepared and characterized by solid-state nuclear magnetic resonance (NMR), X-ray powder diffraction (XRD), N_2 adsorption, and temperature programmed desorption (TPD). Samples were pretreated at different temperatures: mild activation at 773 K (treatment 1) and high temperature activation at 823, 873, 973, and 1073 K (treatment 2). The catalysts showed similar catalytic propane reaction rates within the experimental error. On the other hand, catalyst after the treatment 1 showed higher cracking selectivity than dehydrogenation by factor of 2 while the selectivity towards dehydrogenation was enhanced for the catalysts treated at high temperatures (cracking-to-dehydrogenation ratio ~1). The change in selectivity suggests that the generation of different active sites—other than Brønsted acid sites (BAS), typically considered the active sites for hydrocarbon conversion. The SSZ-13-6 treated at 823 and 873 K showed different selectivity without notable change in reactivity and activation energies, compared to the acid catalyst after treatment 1. The SSZ-13-12 after high temperature treatments showed gradually decreasing activation energies and increasing selectivity toward dehydrogenation with pretreatment temperature (from 823 to 1073 K). The result leads to the hypothesis that the different types of new active sites are generated in SSZ-13-12 and SSZ-13-6 samples, respectively.

Introduction

Understanding the effects of post-synthesis zeolite treatments, including high temperature, has been important for improving and modifying the catalytic properties [1-11] of zeolites in general. High-temperature treatment of zeolites, normally above 873 K, leads to the thermal decomposition of Brønsted acid sites (BAS), Si-O(H)-Al, by a process called dehydroxylation [12, 13]. The IR absorption band of the OH-groups of the BAS is detected in the range of 3600 – 3660 cm^{-1} in the IR spectra of dehydrated samples [3, 14], and the concentration of the BAS can be estimated based on the relative intensity of this signal. It has been shown that samples treated at high temperatures have new chemical properties, including their ability to extract electrons from adsorbed species. For example, xanthene, iminostilbene, fluorene, 2,5-dimethylhexa-2,4-diene, biphenyl, and naphthalene [15-18] form radical cations upon adsorption on pretreated zeolites. It is also important to understand the properties of dehydroxylated zeolites because high temperatures are found in important industrial processes, such as in the regenerator of a fluidized catalytic cracking (FCC) unit or in the catalytic converters of automobiles.

In a dry inert atmosphere, there are two mechanisms by which the BAS dehydroxylation can proceed. In the *heterolytic* mechanism, the dehydroxylation proceeds through dehydration of BAS leading to the formation of water and Lewis acid sites (LAS), as illustrated in Scheme 1 [12, 13, 19]. In the *homolytic* mechanism (Scheme 2), the hydrogen atoms of the acid sites are lost as H·, that is hydrogen atoms, leading to the formation of an oxidized species on the zeolite surface. Nash et al. observed the production of hydrogen during dehydroxylation processes [19] corroborates that dehydroxylation could proceed through a homolytic mechanism in high-silica zeolites. The electron deficient sites formed by dehydrogenation of BAS (Scheme 2) can have redox properties that may impact the catalytic properties of the sample [19]. More detailed investigation of the sites generated after dehydroxylation has been difficult because these sites are EPR silent [16] and do not appear to have any well-defined UV/Vis or IR signature. We have shown that the sites that are generated after dehydroxylation have the ability to extract a single electron from a neutral organic molecule, such as naphthalene, forming radical cations [4]. In addition, long-lived electron-hole pairs are formed by migration of electrons from the zeolite framework to the radical cations. This observation suggests that the new sites

could lead to a catalytic activation of adsorbed species by a redox mechanism instead of the typical protolytic mechanism.

The activation of small alkanes has been used frequently as a model reaction, because the cleavage of the C-C and C-H bonds in the hydrocarbon is a problem of both scientific and technological interest. Alkane activation on acid sites in zeolites can proceed through bimolecular and monomolecular pathways. The bimolecular pathway involves hydride transfer between an alkane and an adsorbed carbenium ion when the concentration of surface species is high. In contrast, the monomolecular pathway (protolytic mechanism), involving the formation of alkanium-like ions, [20-28] is kinetically dominant at high temperatures (~773 K), low alkane partial pressure, and low conversion (<2%). The propane reaction rates and selectivity over H-ZSM-5 before and after dehydroxylation were investigated [3], showing comparable catalytic rates for propane activation but different selectivity and different activation energies [3]. In the monomolecular propane reaction, the reaction proceeds only through two channels, i.e., cracking and dehydrogenation. While acid catalysts have higher propane cracking selectivity than dehydrogenation by a factor of about three, the catalysts after dehydroxylation show similar cracking and dehydrogenation rates [3]. Reduced apparent activation energies for cracking (from 184 kJ/mol to 144 kJ/mol) and for dehydrogenation (from 187 kJ/mol to 127 kJ/mol) are also observed [3]. These changes indicate that the new sites catalyze the hydrocarbon conversion through a different reaction mechanism; a redox mechanism is a potential path for the reaction. Deuterium-labeled propane (C_3D_8) was used to evaluate the redox mechanism by measuring relative reaction rates of cracking and dehydrogenation (r_{C3H8}/r_{C3D8}) before and after dehydroxylation [3]. The relative reaction rate of cracking is not affected by the deuterium label, while that of dehydrogenation is increased from 1.13 to 3.5 [3]. This change in the relative reaction rate of dehydrogenation is consistent with radical cation chemistry [23]. The complexity of the ZSM-5 zeolite catalysts (12 distinctive tetrahedral sites) precludes complete understanding of the structure of the active sites. The presence of 12 distinctive T-sites results in different turnover rates for the monomolecular propane conversions [29].

In this report, SSZ-13 (CHA) was used to activate propane because SSZ-13 has only one topologically distinct tetrahedron site and only four non-equivalent oxygen atoms [30, 31] in the structure. SSZ-13 is a promising solid catalyst for the methanol-to-olefins (MTO) process due to its unique shape-selectivity [32-37]. Adsorption capacity of SSZ-13 at ambient temperature and pressure also makes it as a promising adsorbent for CO_2 capture [38]. Copper exchanged SSZ-13 is a promising catalyst for selective catalytic reduction of NOx with ammonia. The Cu-SSZ-13 has high activity for NH_3-SCR and shows high nitrogen formation selectivity [39, 40].

We report the catalytic reaction rates and selectivity over SSZ-13 with different Si/Al ratios (6 and 12) after thermal treatments for the monomolecular propane reaction. The samples treated at different temperatures were characterized by XRD, N_2 adsorption isotherm, TPD, and ^{27}Al and ^{29}Si solid-state NMR. The product-distribution and the kinetic analysis indicate that different types of active sites are generated by thermal treatments. The catalytic properties of newly generated sites are also different for the samples with different Si/Al ratios. In case of SSZ-13-6, the selectivity has changed dramatically with just 50 K of change in the treatment temperature from 773 K to 823 K, which is "normal" calcination temperature for acid zeolites prior to reaction tests. The activation energy does not change despite this drastic selectivity change. In case of SSZ-13-12, the selectivity and activation energy changed gradually with the treatment temperature, indicating generation of different active sites after thermal treatments. Further work is still necessary to establish the molecular structure of these new sites.

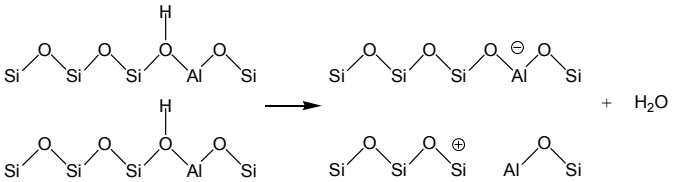

Scheme 1: Dehydroxylation of Brønsted acid sites by dehydration

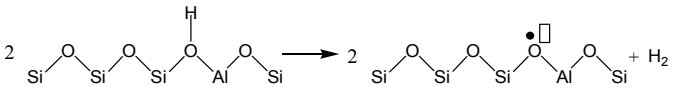

Scheme 2: Dehydroxylation of Brønsted acid sites by dehydrogenation

Experimental Section

Synthesis of SSZ-13

SSZ-13 samples are synthesized using N,N,N-trimethyl-1-adamantanammonium ion ($TMAda^+$) as a structure directing agent (SDA). Two different methods are used to prepare the SSZ-13 samples with different Si/Al ratio. SSZ-13 with low Si/Al ratio (SSZ-13-6, Si/Al ~ 6) is synthesized using a procedure reported by Zones [38, 41]. In this procedure 20 g of sodium silicate (Na_2O_3Si, Sigma Aldrich) and 0.64 g sodium hydroxide (NaOH, Fisher Scientific) are mixed with 48 g of deionized water at room temperature for 15 min. Next, 2 g of NH_4-Y zeolite (Zeolyst CBV-100) is added to the solution and stirred for 30 min. This is followed by the addition of 8.4 g of TMAdaOH (SACHEM Inc., 25% aqueous solution) to the solution and mixing for another 30 min in a covered container. The hydrothermal conversion of the synthesis solutions is carried out in Teflon-lined Parr autoclaves at a temperature of 413 K under rotation for 6 days. The zeolite samples are separated from the solution using vacuum filtration, washed using deionized water, and dried at room temperature. The as-synthesized zeolites are calcined in air at 823 K with 2 K/min heating rate for 8 h to remove the occluded $TMAda^+$.

The synthesis method of SSZ-13 with high Si/Al ratio (SSZ-13-12, Si/Al = ~ 12) is also based on the report written by Zones [42] and by Eilertsen et al. [43] 13 g of tetraethyl orthosilicate (TEOS, Sigma Aldrich) and 26.4 g of TMAdaOH are mixed with 2.7 g of water at room temperature. The solution is stirred

for 2 h and then 0.7 g of aluminum ethoxide ($Al(C_2H_5O)_3$, Sigma Aldrich) is added and mixed for additional 1 h. The resulting solution is then hydrothermally treated in Teflon-lined Parr autoclaves at 413 K under static condition for 6 days. Sample filtration, washing, drying, and calcinations are identical to those of SSZ-13-6 sample.

Analytical

X-ray powder diffraction (XRD) patterns were collected on a Phillps X'Pert X-ray diffractometer using a CuKα radiation. EDX spectral analysis integrated in JEOL JSM 7400F scanning electron microscope (SEM) was used to determine the composition of the samples. The micropore volumes of samples were determined using N_2 adsorption isotherms measured by using a Micromeritics ASAP 2020 instrument. The samples were degassed at 623 K for one day using an in-house-built silica tube. The adsorption isotherms were obtained for the acid form of the samples and the dehydroxylated samples.

Ammonia temperature programmed desorption (TPD) was measured by using a catalyst characterization system (Altamira Instrument AMI-200iρ). About 30 mg of the sample was loaded in a quartz U-tube reactor and the first TPD experiment was carried out by heating the sample to 773 K with a ramping rate of 10 K/min. The acid form of the sample was obtained after this treatment. The ammonium form of the sample was restored by exposing to NH_3 flow for 30 min at 373 K, and then, the TCD signal was recorded up to 800 K. For the thermally treated catalyst, the sample was first heated to 1073 K (and 873 K for SSZ-13-6) at a ramp rate of 10 K/min, cooled down, exposed to NH_3 flow for 30 min at 373 K, and then, the TCD signal was recorded up to 800 K.

^{27}Al and ^{29}Si NMR experiments were recorded on a Bruker AVIII-500 solid-state NMR spectrometer, operating at a Larmor frequency of 500.138 MHz for ^{1}H and 99.362 MHz for ^{29}Si. A 4 mm HX MAS probe was used for all measurements. All spectra were collected at a MAS frequency of 10 kHz, controlled to with +/- 2Hz using a Bruker MAS controller. ^{29}Si single pulse and cross polarization (CP) experiments were performed on each sample. For ^{29}Si single pulse MAS experiments, a 90 degree pulse with a width of 4.3 μs was used and the recycle delay was 30 s. For ^{1}H-^{29}Si CP MAS experiment, ^{1}H 90° pulse duration was 2.5 μs, a linear amplitude ramp (80~100 %) on ^{1}H was used with a contact time of 4.5 μs, and the recycle delay was 5 s. For ^{27}Al MAS with and without proton high-power decoupling, a pulse with a width of 1.35 μs was used and the recycle delay was 1 s.

Thermal Treatment of Zeolite and Catalysis

The samples were treated in the quartz plug flow reactor (ID = 5 mm). To support the sample in the center of the reactor, quartz wool was placed near the bottom of the reactor tube and quartz chips were located between quartz wool and the sample. The reactor was heated using a cylindrical furnace (C5232, Hoskins MFG. CO.) and the temperature was managed using a temperature controller (NC 74000, Omega Engineering). Treatment protocols for the treatments 1 and 2 were illustrated in Figure 1. The zeolites were first heated at 673 K for 2 h to remove water in the samples. To obtain acid catalysts, the samples were then heated at 773 K for additional 3 h (treatment 1, solid black line). The other thermally treated catalysts were prepared by heating the samples once again at 823, 873, 973 (dashed grey lines), or 1073 K for 1.5 h (1073 K - treatment 2, solid grey line). After treatments, the reaction temperatures varied from 733 K to 803 K. The flow rate of the reactant gas, which contains 5 mole % of propane (Matheson tri-gas, research grade) diluted in N_2, was fixed to 80 sccm. The conversion was kept low under 2 % for the monomolecular propane reaction. The product distribution was collected by using a gas chromatography (GC, Shimadzu 2014). A thermal conductivity detector (TCD) and a flame ionization detector (FID) were used to detect hydrogen and hydrocarbons, respectively.

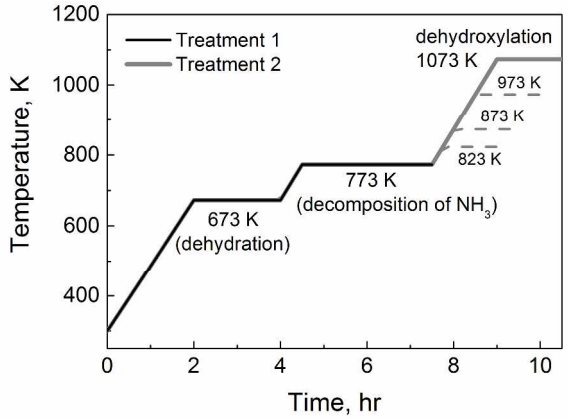

Figure 1. Temperature protocols for two treatments; 1) treatment 1 for acid catalyst and 2) treatment 2 for dehydroxylated catalyst

Results and Discussion

Effect of Treatment on the Structure of the Sample

XRD and N2 adsorption analysis The XRD patterns for the samples with two different Si/Al ratios indicated that the calcined SSZ-13 samples (treatment 1) have high crystallinity (Figure 2) and are free of any crystalline or amorphous impurities. The full widths at half maximum (FWHM) of the (-210) and (-311) reflections (2θ = 20.6° and 30.7°, respectively) were 0.21° and 0.26° for SSZ-13-12 after treatment1. The FWHM of (-210) reflection did not change, while the (-311) reflection FWHM increased by approximately 11 % (from 0.26° to 0.29°) after treatment 2. However, the SSZ-13-12 sample was still highly crystalline after treatment 2, because structural damage and amorphous phase (background) other than slightly-broadened XRD peaks were not observed. Conversely, the XRD pattern of the SSZ-13-6 sample after treatment 2 showed reduced peak intensities and reveals the presence of a (minor) amorphous phase in the background, while the XRD pattern of the SSZ-13-6 treated at 873 K was still highly crystalline. The

FWHM of the (-210) reflection (2θ = 20.7 °) for SSZ-13-6 increased stepwise, i.e., from 0.18° to 0.19°, from 0.19° to 0.20°, and 0.20° to 0.24° as the treatment temperature increased from 773 K (treatment 1) to 873K, from 873K to 973 K, and from 973 K to 1073 K (treatment 2), respectively. The FWHM of the (-311) reflection (2θ = 20.7°) for SSZ-13-6 also increased from 0.26 to 0.29, from 0.29 to 0.31, and from 0.31 to 0.33. The effective particle size of crystal, calculated using the ##Scherrer equation [44], of the (-210) reflection for SSZ-13-6 decreased from 46.9 to 44.4, from 44.4 to 42.2, and from 42.2 to 35.1 nm as the treatment temperatures increased from 773 K (treatment 1) to 873K, to 973 K, and to 1073 K (treatment 2).

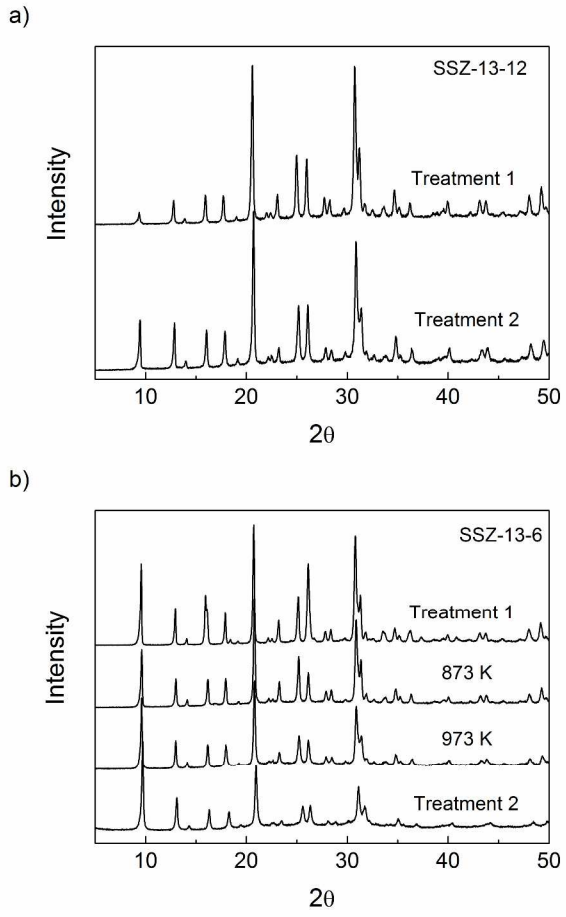

Figure 2. XRD patterns of (a) H-SSZ-13-12 and (b) H-SSZ-13-6 : calcined vs. thermally treated ones

Table 1. Micropore volumes (cm^3/g)

Treatment protocol	H-SSZ-13-12	H-SSZ-13-6
Treatment 1	0.257	0.275
Treated at 873 K	-	0.274
Treated at 973 K	-	0.192
Treatment 2	0.240	0.178

The micropore volumes of H-SSZ-13-12 and H-SSZ-13-6 after treatment 1 were 0.25 cm^3/g and 0.27 cm^3/g, respectively, showing good agreement with the expected values based on the chabazite structure and previous reports [45]. Table 1 shows that the volume of micropores in SSZ-13-12 decreased by 5% after treatment 2; there was no substantial structural damage even if the decomposition of BAS led to the minor reduction of the volume of the micropores. After heating the SSZ-13-6 sample to 873 K, the microporous volume did not decrease, but after heating the SSZ-13-6 samples to 973 K and 1073 K (treatment 2), there was significant reduction in the microporous volume, which is evidence of structural damage. XRD analysis and N_2 adsorption analysis show then that the sample with Si/Al ratio of 6 (SSZ-13-6) is less thermally stable and reveal some collapse of the crystalline structure at temperatures over 973 K. Consequently, the maximal treatment temperatures were 873 K for the SSZ-13-6 and 1073 K for the SSZ-13-12.

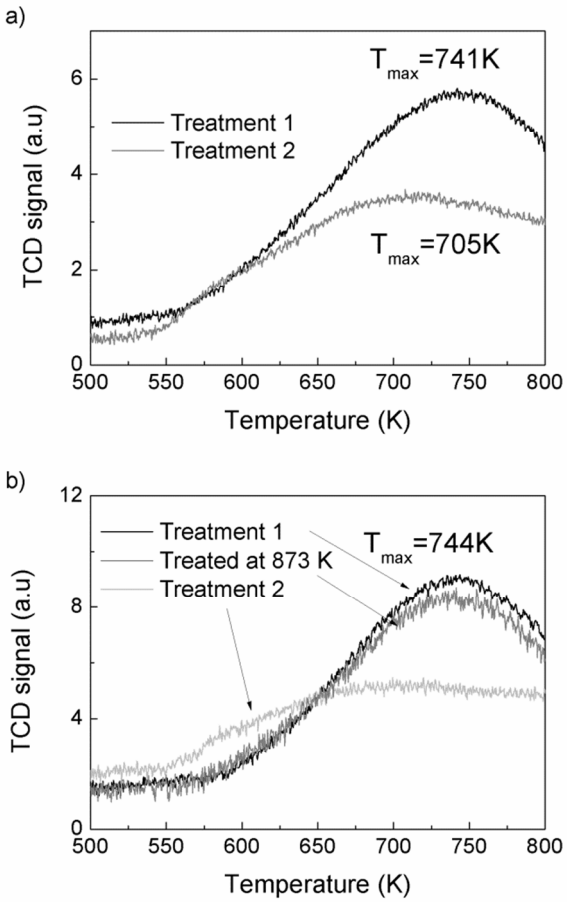

Figure 3. Ammonia TPD for (a) SSZ-13-12 after treatments 1 (black) and 2 (grey), and (b) SSZ-13-6 after treatment 1 (black), treated at 873 K (grey), and after treatment 2 (light grey)

Ammonium TPD experiment The thermal conductivity detector (TCD) signal profiles of ammonium desorption from the samples are illustrated in Figure 3. After treatment 2, the amount of ammonia desorbed clearly decreases on SSZ-13-12 (Figure 3(a)); a large fraction of the Brønsted acid sites

involved in ammonia adsorption was destroyed by heating to 1073 K. In addition, the position of the peak maximum in the signal profile shifted to a lower temperature from 741 K to 705 K. The temperature of the peak maximum is affected by the number of acid sites in the zeolite, the change in the zeolite structure, the carrier gas flow rate, or the amount of the sample [46]. Thus, the reduction of peak maximum temperature reflects a smaller number of acid sites after treatment 2. It has been also reported that ZSM-5 after thermal dehydroxylation at 1093 K exhibited much lower TCD trace than ZSM-5 treated at 823 K [3], similarly indicating a reduction in the number of BAS during dehydroxylation and the formation of non- or weakly interacting sites with ammonia. The sites produced in SSZ-13-12 sample by treatment 2 are then only mildly acid and do not strongly adsorb ammonia. For SSZ-13-6, the TCD signal of the sample treated at 873 K did not significantly change after treatment at 873 K (Figure 3(b)). The amount of ammonia desorbed decreased after treatment 2 due to dehydroxylation or structural damage and the position of the peak maximum cannot be determined.

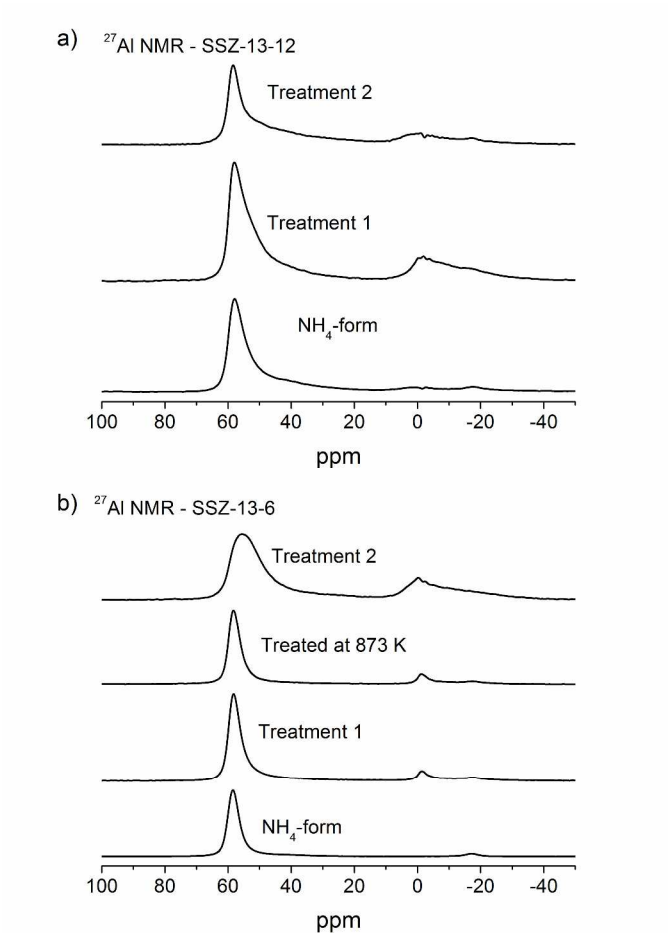

Figure 4. ^{27}Al NMR of a) SSZ-13-12 samples; NH_4-form, treated at 773 K and 1073 K, b) SSZ-13-6 samples; NH_4-form, treated at 773 K, 873 K, and 1073 K.

Solid-state ^{27}Al and ^{29}Si MAS NMR analysis The local structure of aluminum species in zeolites can be determined using ^{27}Al MAS NMR measurements (Figure 4). The resonance band at around 60 ppm is assigned to the Al atoms in tetrahedral coordination, and the additional band around 0 ppm is normally assigned to extraframework Al in octahedral coordination [47-52]. Figure 4 shows that the NH_4-form of SSZ-13-12 has predominantly tetrahedral Al sites. Extraframework octahedral Al sites were generated in SSZ-13-12 sample after treatment 1, but this fraction decreased after treatment 2. A broad band was detected between 50 and 40 ppm in SSZ-13-12 after treatment 2. This broad band is related to extraframework pent-coordinated Al sites. The extraframework Al sites can be related to dealumination of the samples [49, 52]. SSZ-13-6 sample also showed the peak at 60 ppm in the NH_4-form, and a peak at around 0 ppm was generated after thermal treatments. The peak at ~60 ppm becomes quite broad and the fraction of extraframework octahedral Al sites increases after treatment 2.

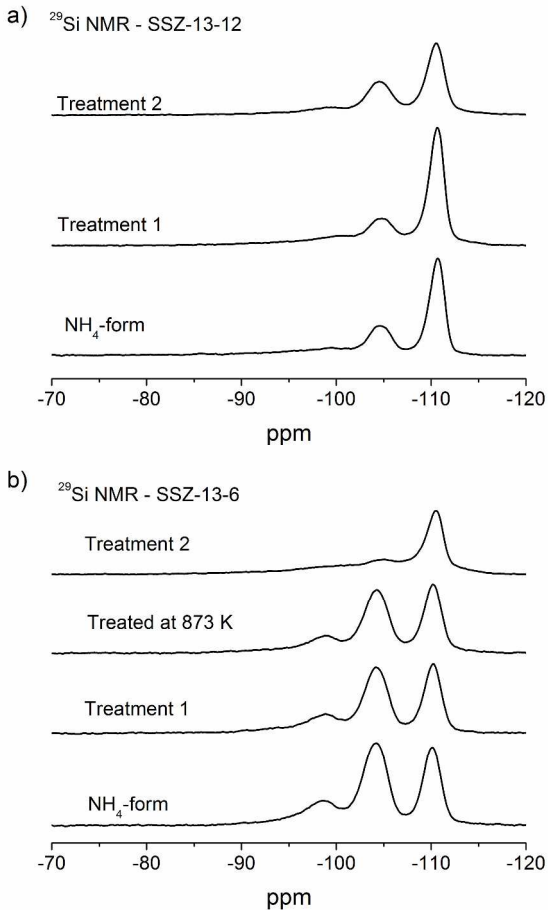

Figure 5. ^{29}Si NMR of a) SSZ-13-12 samples; NH_4-form, treated at 773 K and 1073 K, b) SSZ-13-6 samples; NH_4-form, treated at 773 K, 873 K, and 1073 K.

^{29}Si MAS NMR spectra of NH_4-form and thermally treated samples are depicted in Figure 5. The three different resonances are assigned to the different Si(nAl) environments. The resonances at around -110 ppm, -104 ppm, and -98 ppm are related to Si4, Si3Al1, and Si2Al2 sites, respectively [47, 48, 53]. The Si/Al compositions of the crystalline framework can be estimated from the relationship;

$$Si / Al = \sum I_{Si(nAl)} / 0.25 \sum n I_{Si(nAl)} \quad (1)$$

where n = 0 ~ 4, $I_{Si(nAl)}$ is the area of the peak for the Si environment. The estimated Si/Al ratios of SSZ-13-12 samples were 13.1, 12.1, and 12.2 for NH_4-form of sample, the sample after treatment 1, and the sample after treatment 2, respectively (Table 2). The Si/Al ratios show little reduction with increments in treatment temperature, but the ratios are in a reasonable range of batch composition of the synthesis procedure. The Si/Al ratios of the SSZ-13-6 sample after treatment 1 and after treated at 873 K were all 6.4, almost same as the ratio of NH_4-form SSZ-13-6. However, the Si/Al ratio for the SSZ-13-6 sample after treatment 2 increases to 10.9 (Table 2), indicating that framework Al atoms are lost after the treatment. From ^{27}Al MAS NMR measurements, the increase of Si/Al ratio of the sample after treatment 2 can be related to the generation of extraframework octahedral Al sites. At the same time, the increase in Si/Al ratio could be related to the structural damage of the framework of SSZ-13-6 sample because of low thermal stability.

Table 2. Normalized relative peak area from the ^{29}Si MAS NMR of SSZ-13 samples

	Treatment	Si4	Si3Al1	Si2Al2	Si/Al ratio
SSZ-13-12	NH_4-form	0.73	0.24	0.03	13.1
	Treatment 1	0.68	0.31	0.01	12.1
	Treatment 2	0.69	0.30	0.02	12.2
SSZ-13-6	NH_4-form	0.42	0.52	0.07	6.2
	Treatment 1	0.44	0.49	0.07	6.4
	Treated at 873 K	0.44	0.49	0.06	6.4
	Treatment 2	0.66	0.32	0.02	10.9

Effect of Treatment Temperature on the Monomolecular Propane Reaction

Reaction rates and selectivity The SSZ-13-12 samples were treated at five different temperatures; 773 K (treatment 1), and 823 K, 873 K, 973 K, and 1073 K (treatment 2). After being treated at temperatures above 873 K, the samples showed very high initial reaction rates of propane, an early period of deactivation, and then stabilization. In contrast, reaction rates were stable for the catalyst treated at 773 K only. For the samples treated at higher temperatures, reaction rates were recorded after the rates became stable. Conversions under 2% indicate that the reactions were performed under differential conditions; this is also verified by the stoichiometric ratio of methane to ethylene for cracking channel and of hydrogen to propylene for dehydrogenation channel. Figure 6 shows the reaction rates of the cracking and the dehydrogenation channels at the reaction temperature of 773 K over SSZ-13-12 and SSZ-13-6 samples treated at different temperatures. The acid form of SSZ-13-12 (after treatment 1) showed higher reaction rates for the cracking channel (0.40 mol/s/g-cat $\times 10^7$) than for the dehydrogenation channel (0.17 mol/s/g-cat $\times 10^7$) and a cracking-to-dehydrogenation ratio of ~2.39 (Table 3).

The total reaction rates over the SSZ-13-12 samples treated at 823, 873, 973, and 1073 K were similar to the reaction rates observed over the SSZ-13-12 after treatment 1 (773 K), despite of a slight increase in reaction rates over the sample treated at 823 K. Earlier reports [3, 4] and the TPD experiment reported above (Figure 3) have found that the number of BAS decreases by dehydroxylation. It is notable that reaction rates of SSZ-13-12 after thermal treatments are similar to the rates of the samples treated at low temperature. This implies that new active sites, different from BAS, can be generated and can catalyze the propane conversion. The cracking and dehydrogenation selectivity showed noticeable changes even though the total reaction rates over SSZ-13-12 samples treated at different temperatures barely changed. For the SSZ-13-12 samples, dehydrogenation selectivity increases step by step as the treatment temperature increases, and the reaction rates of the dehydrogenation channel become identical to the reaction rates of the cracking (0.32 mol/s/g-cat $\times 10^7$) at 973 K. It can be assumed that the proportion of sites different from BAS increases stepwise with treatment temperature, and that the mechanism of reaction changed beginning at the temperature of 973 K.

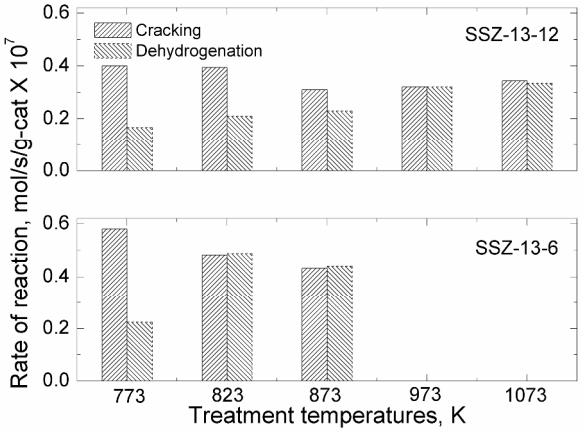

Figure 6. Reaction rates for cracking and dehydrogenation of propane at reaction temperature 773 K over SSZ-13-12 and SSZ-13-6 treated at different pretreatment temperatures.

Table 3. Cracking-to-dehydrogenation ratios at reaction temperature 773 K for SSZ-13-12 and SSZ-13-6 treated at different temperatures.

Treatment Temp., K	773 (Treatment 1)	823	873	973	1073 (Treatment 2)
SSZ-13-12	2.39	1.88	1.35	1.00	1.03
SSZ-13-6	2.59	0.99	0.98	-	-

SSZ-13-6 samples were treated at 773 (treatment 1), 823, and 873 K. The temperatures of 973 and 1073 K were not employed because of the samples low thermal stability as discussed above. The acid form of SSZ-13-6 (after treatment 1) also showed higher reaction rates for the cracking (0.58 mol/s/g-cat ×107) than for dehydrogenation (0.22 mol/s/g-cat ×107), resulting in cracking-to-dehydrogenation ratios ~2.59 (Table 3). The SSZ-13-6 treated at 823 exhibited a little higher total reaction rate, and the SSZ-13-6 treated at 873 K showed similar total reaction rates, compared to that over the SSZ-13-6 after treatment 1 (773 K). The SSZ-13-6 samples showed very low reaction rates after treatment at 973 K and 1073 K (data not shown), as expected given that their structure was damaged by the treatment (see above).

The SSZ-13-6 samples showed drastic changes in selectivity with small change of treatment temperatures. After a pretreatment temperature of 823 K, the cracking-to-dehydrogenation ratio decreased from 2.59 to 0.99 with just 50-degree increase in the treatment temperature (Table 3). This drastic change in selectivity without apparent decomposition of BAS (as shown by the ammonia TPD experiments) cannot be explained at this time.

In Figure 7, the reaction rates of cracking and dehydrogenation over SSZ-13-12 and SSZ-13-6 were compared for pretreatment temperatures of 773 K and for the respective highest treatment temperatures (1073 K for SSZ-13-12 and 873 K for SSZ-13-6). The cracking rates decreased slightly after thermal treatment for both samples, but dehydrogenation rates were significantly increased. Note that the change in selectivity after complete dehydroxylation is similar for both samples even if the treatment temperatures for SSZ-13-12 and SSZ-13-6 are different.

Reaction mechanism The reaction rates and selectivity patterns suggest that the reaction mechanism on the pretreated SSZ-13 samples is different from the typical protolytic mechanism on the acid catalysts (treatment 1). An identical trend of selectivity change of the propane reaction over H-ZSM-5, before and after dehydroxylation, has been reported [3]. The formation of redox sites and Lewis acid sites has a role in the reactivity and selectivity of the zeolite samples [3] and that these sites have the ability to extract electrons from neutral organic materials, such as naphthalene [4].

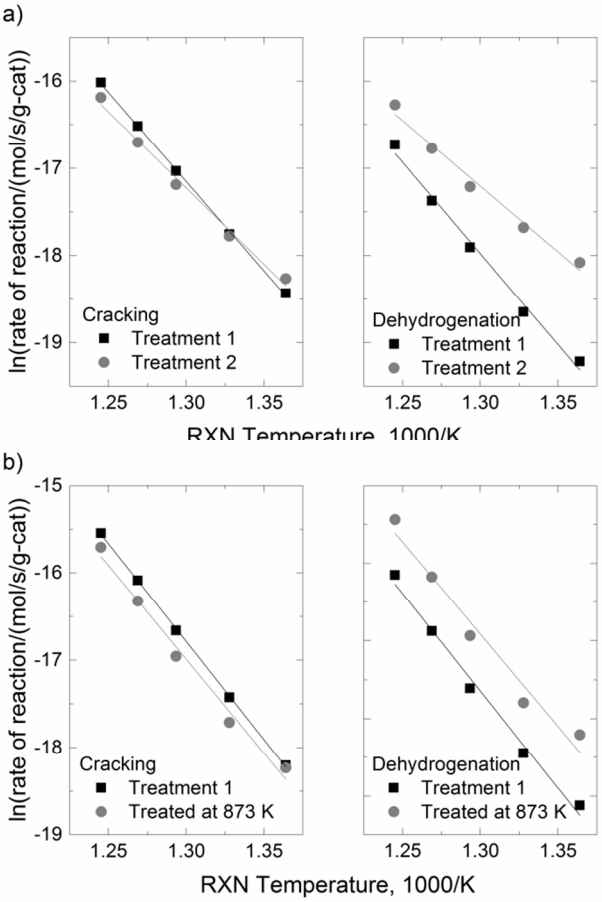

Figure 7. Log scale reaction rates for cracking and dehydrogenation of propane over a) SSZ-13-12 after the treatments 1 and 2 and b) SSZ-13-6 after treatment 1 and treated at 873 K.

A kinetic analysis of the data has been carried out by using following relationships:

$$r = k_3 \frac{K_1 P_{C_3H_8}}{1 + K_1 P_{C_3H_8} + K_4^{"} P_{C_3H_6} + K_4^{'} P_{C_2H_4}} \quad (2)$$

$$r = k_3 K_1 P_{C_3H_8} = k_{app} P_{C_3H_8} \quad (3)$$

Under the conditions for monomolecular propane reaction, such as low partial pressure, low conversion, and high reaction temperatures, the rate expression can be simplified to a first-order rate equation (Eq. 3). The measured activation energies are reported in Table 4. For H-SSZ-13-12 after treatment 1, the activation energy for cracking is 170 kJ/mol, a little lower than that for dehydrogenation (174 kJ/mol). H-SSZ-13-6 after treatment 1 also exhibited higher activation energy for dehydrogenation (208 kJ/mol) than that for cracking (179 kJ/mol). A higher activation barrier is expected for dehydrogenation than for cracking because of the relative stabilities of the protonated C-H and C-C bonds in the propane molecule [30]. The difference of the activation energy ($E_{a,meas}$ for cracking < $E_{a,meas}$ for dehydrogenation) for the acid catalyst was consistent with previous reports. At the same time, the

activation energy values showed good agreement with the experimental values for ZSM-5 samples [3, 23] and the values determined from the simulation of the propane reaction over the acidic chabazite [53, 54].

The activation energy for SSZ-13-12 samples shows a stepwise decrease as the treatment temperatures increased (146 kJ/mol and 114 kJ/mol, for cracking and dehydrogenation, respectively), consistent with the change in selectivity. For the SSZ-13-12 after treatment 2, the activation energy for cracking was greater than that for dehydrogenation. The differences in activation energy indicate that the different intermediates are generated during the propane conversion on the SSZ-13-12 sample after treatment 2 compared to the sample after treatment 1. The NMR and ammonium TPD experiments indicate that the selectivity change in SSZ-13-12 is related to decomposition of BAS. In a previous report, different activation energies were also observed for propane conversion over ZSM-5 before and after thermal treatments [3]. It was suggested that redox sites are generated in ZSM-5 after dehydroxylation, the sites that can extract an electron from neutral adsorbed molecules [3]. Here, the activation energy for SSZ-13-12 was significantly lower after the treatment 2, as in the ZSM-5 case. We conclude that new sites must be generated by the thermal treatment and their effect increases as the treatment temperature increases because more BAS are decomposed. Consequently, the properties of the thermally treated catalysts lead to greater selectivity for the dehydrogenation channel in the propane conversion.

Table 4. Measured activation energies for SSZ-13-12 and SSZ-13-6 treated at different temperatures.

Treatment Temp., K	Measured activation energy, $E_{a,meas}$ (kJ/mol)			
	SSZ-13-12		SSZ-13-6	
	Cracking	Dehydrogenation	Cracking	Dehydrogenation
773 (treatment 1)	170	174	179	208
823	170	161	178	206
873	165	158	179	198
973	114	84		
1073 (treatment 2)	146	114		

The proposed redox catalytic cycle over dehydroxylated SSZ-13-12 sample is depicted in Scheme 3. An electron is extracted from the propane molecule, resulting in the formation of a propane radical cation. The propane radical cation then dissociates into the propylene radical cation with hydrogen, or the ethylene radical cation with methane. The reaction cycle is completed after the electron is given back to the propylene or ethylene radical cations. Note that activation energy at the treatment temperature of 973 K is exceptionally lower than the values observed at other temperatures. It is possible that 1) some new sites, which have the different ability of the catalytic reaction than redox sites or LAS, were generated at 973 K but disappeared at 1073 K, and 2) some specific portion of the newly-generated sites may affect high dehydrogenation selectivity and the kinetics of the reaction.

The activation energies of SSZ-13-6 treated at 823 K were indistinguishable from those of SSZ-13-6 after treatment 1 (the acid catalyst). The activation energy of the dehydrogenation reaction decreased by ~10 kJ/mol (208 kJ/mol for SSZ-13-6 after treatment 1 to 198 kJ/mol for SSZ-13-6 treated at 873 K), while the values of the cracking reaction did not change. At this time the molecular origin of this change in selectivity is not clear. It may be that only a small number of new dehydrogenation sites are formed given that the ammonia TPD traces are nearly unchanged and that the change in selectivity reflects the contributions of these sites.

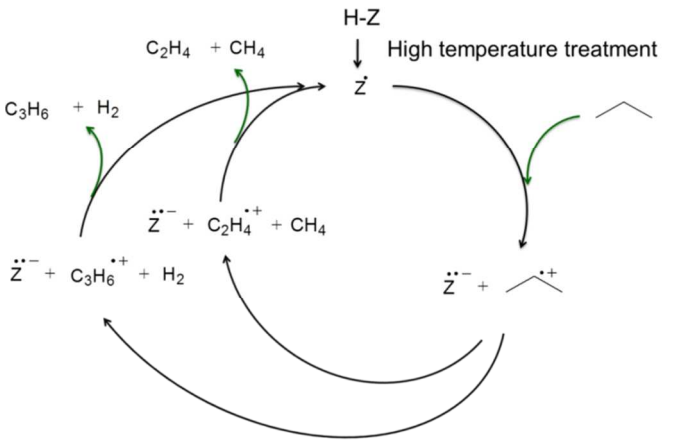

Scheme 3: Redox catalytic cycle for propane conversion over zeolite after high temperature treatment

Conclusions

The structure-activity relationship of the SSZ-13 samples after thermal treatments is summarized in Table 5. Low thermal stability of SSZ-13-6 limited the pretreatment temperature to a maximum of 873 K. Therefore, thermal decomposition of BAS was not observed in the SSZ-13-6 sample at given treatment temperatures (823 and 873 K) even if the heterolytic mechanism is expected to be predominant due to locations of BAS close to each other. Instead, structural damage was observed for the samples after treated over 873 K. The reaction rates of the propane conversion were similar for the acid catalyst and the thermally treated catalysts. However, SSZ-13-6 treated at 873 K showed higher selectivity in the dehydrogenation but the identical kinetic parameters. The observed results indicate that the selectivity change is not result of generation of LAS or redox sites and the change in cell volume after thermal treatment may lead to the confinement effect, promoting C-H cleavage. Different measured activation energies were observed for the SSZ-13-12 sample treated at 1073 K despite of higher selectivity in dehydrogenation channel. The decreased activation energies and change in selectivity suggest the generation of different active sites, other than BAS, in SSZ-13-12. After thermal treatments, LAS and the redox

sites can be generated and could play an important role in the catalytic activity in the SSZ-13-12 sample. The observations in this work confirm the existence of different active sites other than BAS and their role of the catalytic activity in hydrocarbon conversion.

Table 5. Summary of effect of treatment temperatures on SSZ-13 samples

	SSZ-13-12		SSZ-13-6	
Structure change with increase in treatment temperature	< 973 K	Partial dehydroxylation	< 973 K	Not changed
	≥ 973 K	Complete dehydroxylation	≥ 973 K	Structural damage
Selectivity change	Gradually (773 to 973 K)		Drastically (773 to 823 K)	
Activation energy change	Decrease gradually		Not changed	
Assumed generated sites	Redox sites (electron deficient sites) & Lewis acid sites		New sites Structural damage (≥ 973 K)	

Acknowledgements
This work is funded by National Science Foundation under Grant Number NSF-CBET-0931059.

Notes and references
[a] Center for Catalytic Science and Technology, Department of Chemical & Biomolecular Engineering, University of Delaware, Newark DE 19716 USA
E-mail: lobo@udel.edu

1. G. T. Kerr, *Journal of Catalysis*, 1969, **15**, 200-&.
2. G. T. Kerr, *Journal of Physical Chemistry*, 1969, **73**, 2780-&.
3. K. A. Al-majnouni, J. H. Yun and R. F. Lobo, *Chemcatchem*, 2011, **3**, 1333-1341.
4. J. H. Yun and R. F. Lobo, *Microporous and Mesoporous Materials*, 2012, **155**, 82-89.
5. V. Valtchev, G. Majano, S. Mintova and J. Perez-Ramirez, *Chemical Society Reviews*, 2013, **42**, 263-290.
6. A. Corma, M. Diaz-Cabanas, J. Martinez-Triguero, F. Rey and J. Rius, *Nature*, 2002, **418**, 514-517.
7. A. Corma, A. Martinez, P. A. Arroyo, J. L. F. Monteiro and E. F. SousaAguiar, *Applied Catalysis a-General*, 1996, **142**, 139-150.
8. J. C. Groen, J. A. Moulijn and J. Perez-Ramirez, *Journal of Materials Chemistry*, 2006, **16**, 2121-2131.
9. J. C. Groen, L. A. A. Peffer and J. Perez-Ramirez, *Microporous and Mesoporous Materials*, 2003, **60**, 1-17.
10. M. Bjorgen, F. Joensen, M. S. Holm, U. Olsbye, K.-P. Lillerud and S. Svelle, *Applied Catalysis a-General*, 2008, **345**, 43-50.
11. P. A. Jacobs, E. M. Flanigen, J. C. Jansen and H. van Bekkum, *Introduction to Zeolite Science and Practice*, Elsevier Science, 2001.
12. Uytterho.Jb, Christne.Lg and W. K. Hall, *Journal of Physical Chemistry*, 1965, **69**, 2117-+.
13. D. N. Stamires and J. Turkevich, *Journal of the American Chemical Society*, 1964, **86**, 749-&.
14. A. Zecchina, S. Bordiga, G. Spoto, D. Scarano, G. Petrini, G. Leofanti, M. Padovan and C. O. Arean, *Journal of the Chemical Society-Faraday Transactions*, 1992, **88**, 2959-2969.
15. H. Garcia and H. D. Roth, *Chemical Reviews*, 2002, **102**, 3947-4007.
16. T. M. Leu and E. Roduner, *Journal of Catalysis*, 2004, **228**, 397-404.
17. M. L. Cano, A. Corma, V. Fornes and H. Garcia, *Journal of Physical Chemistry*, 1995, **99**, 4241-4246.
18. A. Moissette, H. Vezin, I. Gener and C. Bremard, *Journal of Physical Chemistry B*, 2003, **107**, 8935-8945.
19. M. J. Nash, A. M. Shough, D. W. Fickel, D. J. Doren and R. F. Lobo, *Journal of the American Chemical Society*, 2008, **130**, 2460-2462.
20. W. O. Haag, R. M. Lago and P. B. Weisz, *Nature*, 1984, **309**, 589-591.
21. A. M. Rigby, G. J. Kramer and R. A. vanSanten, *Journal of Catalysis*, 1997, **170**, 1-10.
22. A. Corma, P. J. Miguel and A. V. Orchilles, *Journal of Catalysis*, 1994, **145**, 171-180.
23. T. F. Narbeshuber, A. Brait, K. Seshan and J. A. Lercher, *Journal of Catalysis*, 1997, **172**, 127-136.
24. S. M. Sharada, P. M. Zimmerman, A. T. Bell and M. Head-Gordon, *Journal of Physical Chemistry C*, 2013, **117**, 12600-12611.
25. D. C. Tranca, N. Hansen, J. A. Swisher, B. Smit and F. J. Keil, *Journal of Physical Chemistry C*, 2012, **116**, 23408-23417.
26. F. C. Jentoft and B. C. Gates, *Topics in Catalysis*, 1997, **4**, 1-13.
27. S. Kotrel, H. Knozinger and B. C. Gates, *Microporous and Mesoporous Materials*, 2000, **35-6**, 11-20.
28. A. Corma and A. V. Orchilles, *Microporous and Mesoporous Materials*, 2000, **35-6**, 21-30.
29. R. Gounder and E. Iglesia, *Journal of the American Chemical Society*, 2009, **131**, 1958-1971.
30. S. R. Stoyanov, S. Gusarov, S. M. Kuznicki and A. Kovalenko, *Journal of Physical Chemistry C*, 2008, **112**, 6794-6810.
31. C. Lo and B. L. Trout, *Journal of Catalysis*, 2004, **227**, 77-89.
32. F. Bleken, M. Bjorgen, L. Palumbo, S. Bordiga, S. Svelle, K.-P. Lillerud and U. Olsbye, *Topics in Catalysis*, 2009, **52**, 218-228.
33. S. Bordiga, L. Regli, D. Cocina, C. Lamberti, M. Bjørgen and K. P. Lillerud, *The Journal of Physical Chemistry B*, 2005, **109**, 2779-2784.
34. E. A. Eilertsen, S. Bordiga, C. Lamberti, A. Damin, F. Bonino, B. Arstad, S. Svelle, U. Olsbye and K. P. Lillerud, *Chemcatchem*, 2011, **3**, 1869-1871.
35. Q. Zhu, J. N. Kondo, T. Tatsumi, S. Inagaki, R. Ohnuma, Y. Kubota, Y. Shimodaira, H. Kobayashi and K. Domen, *Journal of Physical Chemistry C*, 2007, **111**, 5409-5415.
36. S. J. Kim, H.-G. Jang, J. K. Lee, H.-K. Min, S. B. Hong and G. Seo, *Chemical Communications*, 2011, **47**, 9498-9500.
37. L. Sommer, A. Krivokapic, S. Svelle, K. P. Lillerud, M. Stocker and U. Olsbye, *Journal of Physical Chemistry C*, 2011, **115**, 6521-6530.
38. S. I. Zones, *Journal of the Chemical Society-Faraday Transactions*, 1991, **87**, 3709-3716.
39. D. W. Fickel, E. D'Addio, J. A. Lauterbach and R. F. Lobo, *Applied Catalysis B-Environmental*, 2011, **102**, 441-448.

40. J. H. Kwak, R. G. Tonkyn, D. H. Kim, J. Szanyi and C. H. F. Peden, *Journal of Catalysis*, 2010, **275**, 187-190.
41. D. W. Fickel, J. M. Fedeyko and R. F. Lobo, *Journal of Physical Chemistry C*, 2010, **114**, 1633-1640.
42. , US4544538-A.
43. E. A. Eilertsen, M. Haouas, A. B. Pinar, N. D. Hould, R. F. Lobo, K. P. Lillerud and F. Taulelle, *Chemistry of Materials*, 2012, **24**, 571-578.
44. A. L. Patterson, *Physical Review*, 1939, **56**, 978-982.
45. G. I. Kapustin, T. R. Brueva, A. L. Klyachko, S. Beran and B. Wichterlova, *Applied Catalysis*, 1988, **42**, 239-246.
46. H. Koller and M. Weiss, in *Solid State Nmr*, ed. J. C. C. Chan, 2012, vol. 306, pp. 189-227.
47. J. Klinowski, *Chemical Reviews*, 1991, **91**, 1459-1479.
48. S. Li, A. Zheng, Y. Su, H. Fang, W. Shen, Z. Yu, L. Chen and F. Deng, *Physical Chemistry Chemical Physics*, 2010, **12**, 3895-3903.
49. L. Wu, V. Degirmenci, P. C. M. M. Magusin, N. J. H. G. M. Lousberg and E. J. M. Hensen, *Journal of Catalysis*, 2013, **298**, 27-40.
50. K. A. Thrush and S. M. Kuznicki, *Journal of the Chemical Society-Faraday Transactions*, 1991, **87**, 1031-1035.
51. S. Li, S.-J. Huang, W. Shen, H. Zhang, H. Fang, A. Zheng, S.-B. Liu and F. Deng, *Journal of Physical Chemistry C*, 2008, **112**, 14486-14494.
52. D. E. Akporiaye, I. M. Dahl, H. B. Mostad and R. Wendelbo, *Journal of Physical Chemistry*, 1996, **100**, 4148-4153.
53. T. Bucko, L. Benco, J. Hafner and J. G. Angyan, *Journal of Catalysis*, 2011, **279**, 220-228.
54. T. Bucko and J. Hafner, *Journal of Physics-Condensed Matter*, 2010, **22**.

Figure Abstract